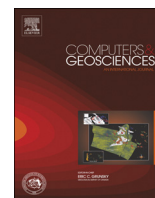




ELSEVIER

Contents lists available at ScienceDirect

Computers & Geosciences

journal homepage: www.elsevier.com/locate/cageo

Research paper

Simulation of non-linear coregionalization models by FFTMA



Min Liang*, Denis Marcotte, Pejman Shamsipour

Department of Civil, Geological and Mining Engineering, École Polytechnique de Montréal, C.P. 6079 Succ. Centre-ville, Montréal (QC), Canada H3C 3A7

ARTICLE INFO

Article history:

Received 6 June 2015

Received in revised form

16 December 2015

Accepted 13 January 2016

Available online 29 January 2016

Keywords:

FFTMA

Multivariate random field

Non-linear model of coregionalization

Unconditional simulation

Conditioning by cokriging

ABSTRACT

A fast and efficient method to simulate multivariate fields with non-linear models of coregionalization (N-LMC) is described. The method generalizes FFTMA to the multivariate simulation of the N-LMC with symmetric cross-covariances, hence the name GFFTMA. It allows us for example to use an exponential model as the direct covariance for the main variable, a Cauchy model for the secondary variable and a K-Bessel model for the cross-covariance. Each covariance and cross-covariance are Fast Fourier Transformed (FFT) to get the discrete spectral densities. Then the spectral matrix is eigen-decomposed at each frequency separately to provide the square root matrix and to enforce positive-definiteness in cases where small negative eigenvalues are found. Finally the simulated spectrum is obtained as multiplication of the root matrix and the white noise coefficients. The method is particularly fast for covariances having derivatives at the origin and/or for covariances with long range. Hence, two-variables' 2D fields of 100 million pixels with all-Gaussian or all-cubic covariances and cross-covariance are both simulated in less than 200 s. The CPU-time increases only as $N \log(N)$ (N , the number of points to simulate). Additional realizations are obtained at a low marginal cost as the eigen-decomposition step needs to be done only once for the first realization. The main limitation of the approach is its rather stringent memory requirement. Synthetic examples illustrate the simulations of N-LMC with two and three variables for different combinations of the seven available models. It shows that the theoretical models are all well reproduced. An illustrative case-study on overburden thickness simulation is provided where the secondary information consists of a latent Gaussian variable identifying the geological domain.

© 2016 Elsevier Ltd. All rights reserved.

1. Introduction

In geology, mining, petroleum, hydrogeology and other applications, it is common to observe several secondary variables that are spatially correlated to the main variable of interest. Often, the secondary variables are more exhaustively sampled than the main variable. To improve precision, it is important to include this information in the simulation of the main variable. Up to now, essentially two cases of figure are encountered in applications. The first one is when a physical relationship exists between the main variable and the secondary ones. This situation is common in geophysics (Asli et al., 2000; Shamsipour et al., 2010, 2011) and in hydrogeology (Ahmed and de Marsily, 1989; Dong, 1990). The second case of figure is the modeling of the statistical link by the linear model of coregionalization (LMC) (Myers, 1983; Marcotte, 1991; Journel and Huijbregts, 1978; Wackernagel, 2003) where it is assumed that all variables being studied share the same spatial structures. Advantages of LMC are important: unequalled ease of

verification of admissibility (Goulard and Voltz, 1992) and possibility to use a large variety of simulation algorithms, including the efficient turning bands' method (Matheron, 1973; Chilès and Delfiner, 2012) and FFTMA (Le Ravalec-Dupin et al., 2000) as all what is required is to combine linearly independent univariate simulations. The main disadvantage of LMC is the rather severe restriction it imposes that the variables share common spatial structures. It is indeed frequent that one observes a smoother behavior on the secondary variables than on the main variable. Using the LMC in this case incurs an important loss of information.

Recently Marcotte (2015) proposed a new tool facilitating the verification of admissibility for non-LMC models (N-LMC) with symmetrical cross-covariances. A direct follow-up is to find an efficient method of simulation of the N-LMC. Shinozuka (1971) developed a continuous spectral method to simulate a multivariate homogeneous process by a series of cosine functions. He proposed to use the Cholesky decomposition of the spectral density matrix, at selected frequencies. Then, the study was extended to non-homogeneous oscillatory processes characterized by an evolutionary power spectrum (Shinozuka and Jan, 1972). Mejía and Rodríguez-Iturbe (1974) focused on discussing connection of correlation and spectrum of a random field and provided a simulation method by sampling from the spectral density functions.

* Corresponding author.

E-mail addresses: min.liang@polymtl.ca (M. Liang), denis.marcotte@polymtl.ca (D. Marcotte).

Zagayevskiy (2015) use the spectral method with turning bands to simulate LMC. Mantoglou (1987) and Emery et al. (2015) implement variants of the continuous spectral method (Shinozuka and Jan, 1972) with turning bands that can both simulate N-LMC.

Alternatively, Pardo-Igúzquiza and Chica-Olmo (1993) developed a Fourier integral method for unconditional simulation of random fields. The FFT was used in both numerical calculations of density spectral function and generation of realizations. Chilès (1995) used the discrete spectral method based on the FFT for simulation of intrinsic random functions. Chilès and Delfiner (1997) propose various tools to simulate by FFT while minimizing aliasing effects due to the asymptotic ranges of many covariance functions. Le Ravalec-Dupin et al. (2000) proposed to integrate FFT and the moving average method in a fast and flexible method they named FFTMA. Applications of FFTMA can be found in Le Ravalec-Dupin et al. (2001), Gloaguen et al. (2005) and Shamsipour et al. (2011). Le Ravalec-Dupin and Da Veiga (2011) extended FFTMA for cosimulation of two variables that are linearly correlated. In addition to being limited to two variables, their method was based on the Markov–Bayes approximation, so it did not allow full control and generality of the simulated cross-covariances.

In this contribution, based on the discrete spectral method, the FFTMA is adapted to the unconditional simulation of multivariate fields with the N-LMC. One requirement on the coregionalization is the cross-covariances must be symmetric. The square root of the spectral matrix is obtained at each frequency sampled by the FFT. Then spectrum of white noise fields for n variables is computed by FFT and combined with the square root matrices (one per frequency) so as to generate the desired direct and cross-structures. To increase the applicability of the FFTMA, we also present a simple idea to extend the simulation to points that do not fall on a regular grid. This allows the post-conditioning by cokriging to be performed to obtain conditional realizations at any desired point.

After reviewing the FFTMA algorithm, we describe the necessary modifications to simulate N-LMC. We then discuss implementation details related to the type of simulated covariance, the admissibility issue, the computing time and the solution proposed for the case of samples not on a regular grid. We show that the program, named GFFTMA, reproduces the desired N-LMC. CPU time and memory requirements are examined. Finally, a case study is presented.

2. Methodology

The moving average method (MA) was presented for simulation of one dimensional Gaussian random fields in Journel (1974). Then, it was extended by Oliver (1995) to two and three dimensions. A zero mean Gaussian random field $z(x)$ with covariance $C(h)$ (h is a distance vector between x_i and x_j) is generated by

$$z(x) = g(h) * y(x), \tag{1}$$

where $*$ is the convolution operator, $y(x)$ is a Gaussian white noise and $g(h)$ is a convolution root of the covariance, i.e. $C(h) = g(h) * \hat{g}(h)$ in which $\hat{g}(h) = g(-h)$. For symmetric covariances and cross-covariances, it is possible to choose $g(h) = g(-h)$, hence a symmetric convolution root g exists (although non-symmetric roots also exist). Oliver (1995) listed covariance functions and their auto-convolution root in two and three dimensions. Le Ravalec-Dupin et al. (2000) recognized the spatial convolution of Eq. (1) is most efficiently computed in the spectral domain by using FFT, hence the method FFTMA was developed. Oliver (2003) described the use of Cholesky decomposition to simulate 2D N-LMC models combining different model types for the direct covariances or different ranges.

The convolution theorem, either in its continuous or discrete versions, states that the Fourier transform of the convolution of two functions is the product of the Fourier transform of the two functions (Cooley et al., 1969; Priestley, 1982; Le Ravalec-Dupin et al., 2000; Rao et al., 2011):

$$\mathcal{F}(g_1 * g_2) = \mathcal{F}(g_1) \cdot \mathcal{F}(g_2). \tag{2}$$

In the univariate case with symmetrical covariance $C = g * g$, where g is the symmetric square root. As the spectral density function $S = \mathcal{F}(C) = \mathcal{F}(g * g) = [\mathcal{F}(g)]^2$, one has $\mathcal{F}(g) = \sqrt{S}$. Thus to obtain the root spectrum, it suffices, in the univariate case, to take the square root of the spectral density function of the covariance. Having the root spectrum, one simply has to multiply it with the spectrum of a Gaussian white noise and then take the inverse Fourier transform to get back in the spatial domain. The final result is the convolution of the covariance root with a Gaussian white noise (a moving average), ensuring correct reproduction of the desired covariances.

2.1. The FFTMA in the multivariate case

Le Ravalec-Dupin and Da Veiga (2011) present an approximate method to simulate sequentially two variables with different structures and a given correlation. Their approach is to simulate a first variable and then to simulate the second one conditional to the first one using a Markov–Bayes hypothesis for the cross-covariance. It is only an approximate method due to the Markov–Bayes hypothesis that does not allow full control on the simulated cross-covariances. For example, when the first variable has a spherical covariance, the second variable could not be simulated exactly with a Gaussian covariance. Here, we seek to generalize the simulation to any number of variables and to allow any covariance and cross-covariance, with the only restriction that the coregionalization must be an admissible model. For this, FFTMA is used to simulate directly the joint distribution of the n variables with imposed covariances and cross-covariances. The idea is based on the fact that knowledge of direct and cross-covariances is equivalent to knowledge of the direct and cross-spectral densities. Hence, the goal is to simulate n variables having completely specified spectral matrices at all frequencies.

The covariance matrix function $C(h)$ is

$$\begin{pmatrix} C_{1,1}(h) & C_{1,2}(h) & \dots & C_{1,n}(h) \\ C_{2,1}(h) & C_{2,2}(h) & \dots & C_{2,n}(h) \\ \vdots & \vdots & \ddots & \vdots \\ C_{n,1}(h) & C_{n,2}(h) & \dots & C_{n,n}(h) \end{pmatrix} \tag{3}$$

Assuming symmetry of cross-covariances, the corresponding spectral matrix $S(f)$ (f is frequency) is obtained by separate Fourier transform of each of the $n \times (n + 1)/2$ covariance functions:

$$\begin{pmatrix} S_{1,1}(f) & S_{1,2}(f) & \dots & S_{1,n}(f) \\ S_{2,1}(f) & S_{2,2}(f) & \dots & S_{2,n}(f) \\ \vdots & \vdots & \ddots & \vdots \\ S_{n,1}(f) & S_{n,2}(f) & \dots & S_{n,n}(f) \end{pmatrix} \tag{4}$$

where $S_{ij}(f) = S_{ji}(f)$ as the Fourier transform of a real even function is also real and even.

At any given frequency f , by Bochner's theorem, the spectral matrix must be positive semi-definite. Then one can use the square root matrix decomposition of $S(f)$ as $S(f) = U(f)U(f)^T$, where T denotes the transpose operator, $U = VD^{1/2}V^T$ and D and V are respectively the diagonal eigenvalue matrix and the orthonormal eigenvector matrix, i.e. one has $S = VDV^T$ and $VV^T = V^TV = I$. Now, consider a zero-mean unit-variance Gaussian white noise $y(x)$ in

the spatial domain. It is well known that its Fourier transform $\tilde{y}(f)$ is also a zero-mean unit-variance Gaussian white noise. Hence, one has

$$E[U(f)\tilde{y}(f)\tilde{y}(f)^T U(f)^T] = U(f)U(f)^T = S(f) \quad (5)$$

where $\tilde{y}(f)$ is a column vector of size n containing the Fourier transform coefficients at frequency f for the corresponding n independent Gaussian white noises. This equation leads to the following algorithm in the discrete case:

- Compute the FFT of each of the $n \times (n + 1)/2$ periodized covariances and cross-covariances evaluated on the regular grid (N points); this provides $S(f)$.
- Generate n independent white noise vectors on N grids and compute their FFT $\tilde{y}(f)$.
- For all frequencies, respectively compute the eigenvalue-eigenvector decomposition of the spectral matrix $S(f)$ and get the $U(f) = V(f)D(f)^{1/2}V(f)^T$. The eigen-decomposition is done on a small matrix of size $n \times n$ at each frequency. For all frequencies, $U(f)$ consists of $n \times n$ matrices.
- Calculate the spectrum of simulation at all frequencies f as $\tilde{z}(f) = U(f)\tilde{y}(f)$.
- Take the separate inverse FFT on each component of vectors $\tilde{z}(f)$ to obtain the simulation $z(x)$ in spatial domain that have the right covariances and cross-covariances.

The reader will note that the above procedure is the direct analog of what is done by FFTMA in the univariate case, where $S(f)$ is a scalar, and one computes $\sqrt{S(f)}\tilde{y}(f)$ and then takes the inverse Fourier transform. In the multivariate case $S(f)$ is a matrix, and the square root is replaced by the square root matrix decomposition. The Cholesky decomposition of $S(f)$ could also have been used, and in fact it was used in the initial versions of GFFTMA. However, it appeared that the Cholesky decomposition was numerically unstable in some models at high frequencies where all the spectral values are close to zero.

2.2. Post-conditioning by cokriging

The classical method of post-conditioning by cokriging (Chilès and Delfiner, 2012) is used, either by simple cokriging or by ordinary kriging or kriging with a trend (Emery, 2007). Therefore,

$$Z_{CS}(x) = Z^*(x) + (Z_S(x) - Z_S^*(x)) \quad (6)$$

where $Z^*(x)$ is the cokriging estimate at simulated point x using the data, $Z_S^*(x)$ is the cokriging estimate at simulated point x using the simulated values at sample points and $Z_S(x)$ are unconditional simulated values obtained with GFFTMA.

An important limitation of the FFTMA is to simulate only on a regular grid. This is a problem for the post-conditioning step as one also needs simulated values at sampled points. Moreover, they must have the right structure and be compatible with all the points already simulated on the regular grid. Relying on the screening effect approximation, one idea is to locally propagate the unconditional simulated vectors of the regular grid to sample points. By the Cholesky or SGS method, values on the sample points can be simulated conditioned by the neighboring regular grid vectors. This is repeated for each sample point in turn. Sample points that are simulated by SGS or Cholesky are added to the already simulated vectors for the next sample points. At the end of the procedure, correlated random vectors with approximately the right covariance structure and compatible with the regular grid are available at each sample point. One can then proceed with the post-conditioning as usual. Note that this step is relatively fast compared to a standard SGS as only the sample points need to be

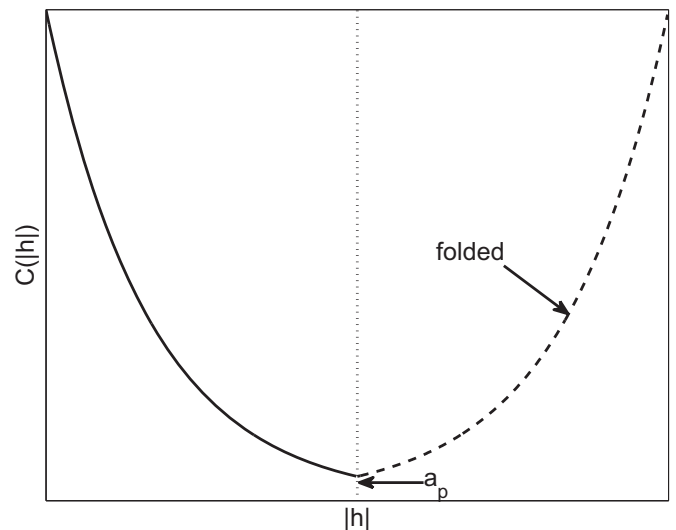


Fig. 1. Example of slope discontinuity at practical range a_p after periodization of the exponential model.

simulated, not the grid points that are already simulated by GFFTMA.

2.3. Models with asymptotic range

Following Le Ravalec-Dupin et al. (2000) and Chilès and Delfiner (2012), the size of the field to simulate internally must be at least $L = b + a$, where b is the size of the desired simulation in a given direction and a is the correlation range in this direction. For covariances that possess only an asymptotic range, the practical range is used (i.e. the distance where the covariance represents only 5% of the sill). One exception is for the Gaussian covariance model where it was found that the practical range was not sufficient to ensure good covariance reproduction at small distances. For this model, the practical range was extended from $\sqrt{3}a$ to $3a$. Note that for all models with asymptotic ranges, the periodicity of the FFT introduces a discontinuity of the slope of the periodized covariances at mid-distance of the simulated field (see Fig. 1). This discontinuity causes the simulated models to become numerically not admissible as some small negative spectral values appear in the spectrum. The solution adopted here is to replace the direct spectral negative values by very small positive values and the corresponding cross-spectral values by zeros. In addition, all negative eigenvalues found during the eigen-decomposition are simply replaced by zeros. This ensures numerical admissibility of each simulated N-LMC. Examples in the next section show that these simple corrections to ensure positive-definiteness at all frequencies of the FFT do not introduce a measurable bias on the covariance. All the simulated covariances and cross-covariances do not depart significantly from the intended theoretical N-LMC.

To account for possible geometric anisotropies in different directions and of covariances formed of multiple nested components, the maximum range or the practical range among all directions and all components of the N-LMC was retained as the unique parameter a used to define the extension of the simulated grid.

2.4. Test of GFFTMA

The examples presented in Figs. 2–5 seek to illustrate the versatility of GFFTMA and the quality of reproduction of the multivariate models. The models are described in detail in Table 1. In each case, 200 realizations of a square field of size 500×500 are obtained for isotropic cases with two variables (Figs. 2 and 3) and

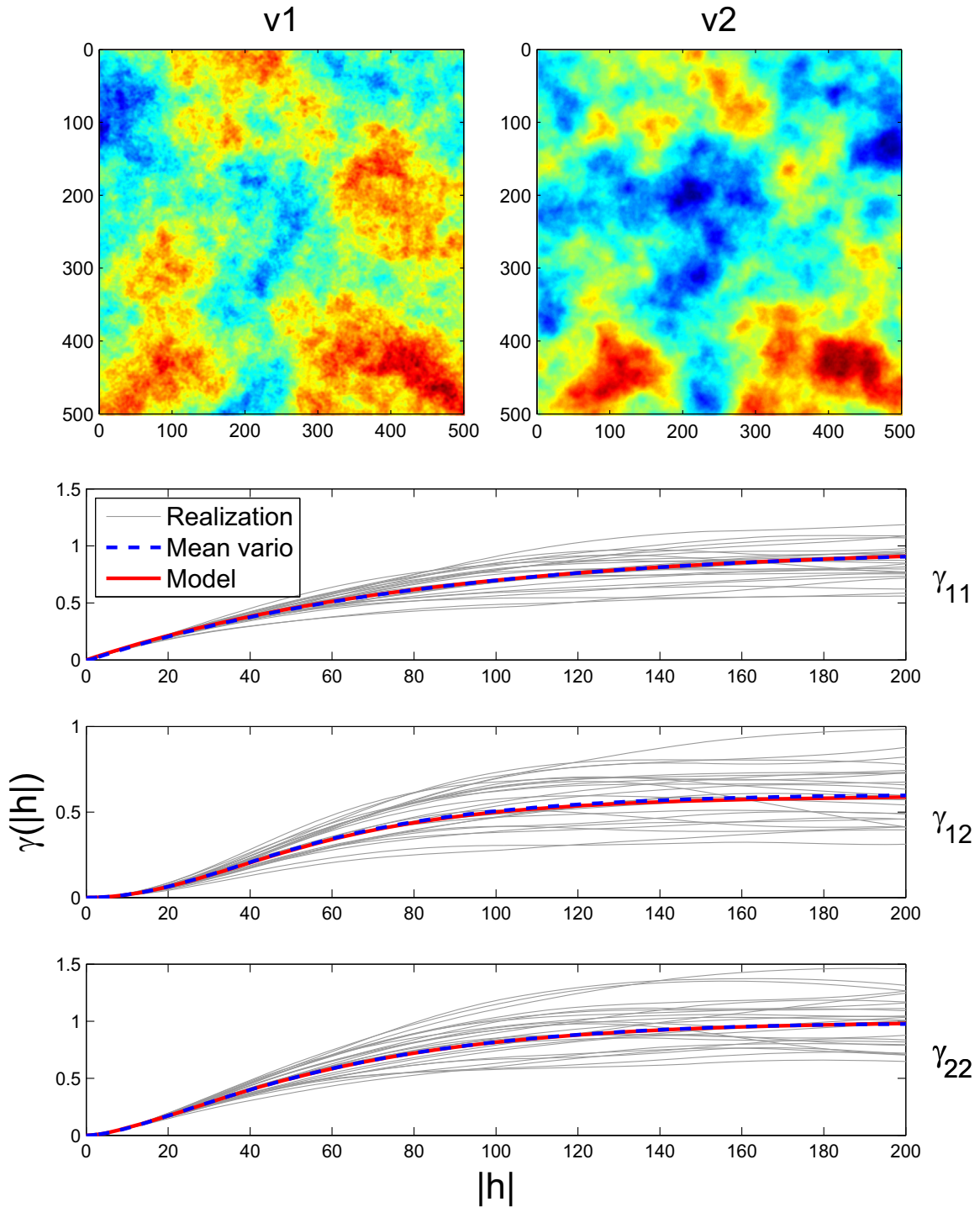


Fig. 2. One realizations of v1 and v2 (top row) and the direct and cross-variograms. Case 1 of Table 1 mixing exponential, Generalized Cauchy with $\nu = 2$ and K-Bessel with $\nu = 1$. Mean variogram is computed by combining E–W and N–S directions over 200 realizations. Only the first 25 individual realization variograms (light gray) are shown.

three variables (Fig. 4) and for an anisotropic case with two variables (Fig. 5). The direct and cross-variograms of the first 25 realizations are illustrated together with the mean variogram computed over the 200 realizations. Models used include mixtures of spherical, exponential, Gaussian, cubic, penta, generalized Cauchy and K-Bessel. The coregonizations are all N-LMC as different structures appear on the direct and cross-variograms. The models are checked to be admissible with program TASC3D (Marcotte, 2015). This program uses the theoretical 3D spectral densities of the same models available in GFFITMA to verify the positive-definiteness of the spectral matrices at any set of user specified

frequencies. It allows any number of components in the direct and cross-covariance models of the N-LMC, each component being isotropic or anisotropic.

2.5. Computing time

Because of the use of FFT, GFFITMA is probably unequaled for the computing time required to get the unconditional simulations. The post-conditioning is generally the slower step, although this step can be also quite fast when dual kriging is used in a global neighborhood (Royer and Vierra, 1984; Davis and Grivet, 1984).

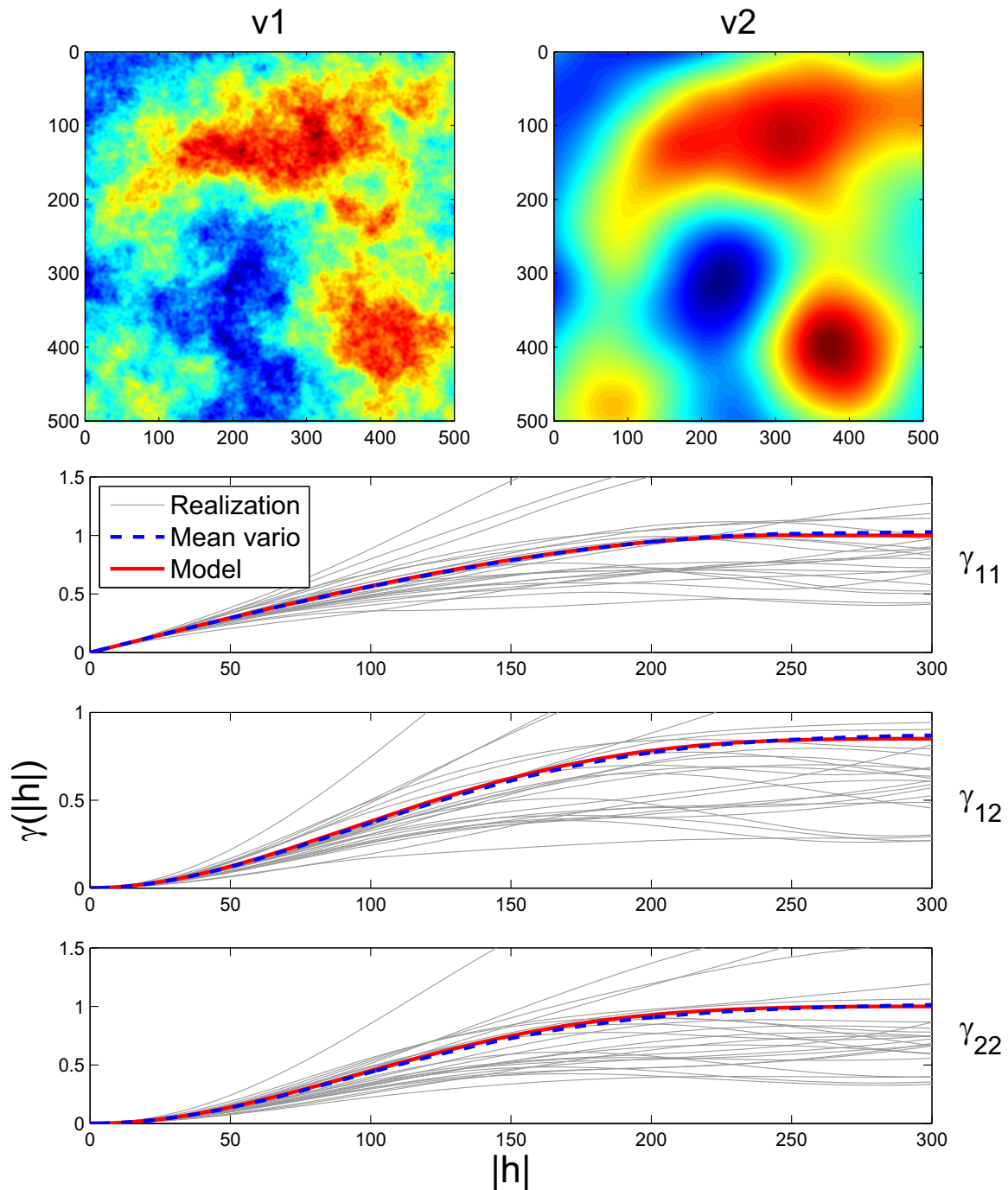


Fig. 3. One realization of v_1 and v_2 (top row) and the direct and cross-variograms. Case 2 of Table 1. Mean variogram is computed by combining E-W and N-S directions over 200 realizations. Only the first 25 individual realization variograms (light gray) are shown.

Fig. 6a shows the well known $N \log(N)$ CPU time relationship of the FFT transform (N is the number of simulated pixels) as the correlation between CPU time and $N \log(N)$ reaches 0.999. Note that one realization for two variables on 100 million pixels is obtained in approximately 200 s for the cubic and Gaussian models with range 100, 500 s for the spherical model with range 200 and 2800 s for the spherical model with range 100 pixels. All computations are done on an Intel Xeon (2.13 GHz). The most consuming computation is the eigen-decomposition. We stress that this computation step is done only once to get the square root matrices. When the model has a linear behavior at the origin and a small range, the eigen-decomposition must be computed at almost all frequencies (which is the total number of pixels in the

simulation). On the contrary, with differentiable variograms at the origin and/or for large range covariances, most frequencies have a quite small contribution that can be disregarded without discernable effects. In all cases, every additional realization is obtained in a comparatively negligible time that is independent of the covariance model used, as each realization calls for only two FFTs and the product of the square root matrices with the Gaussian white noise FFT coefficients. As expected, the simulation time increases linearly with the number of realizations (Fig. 6b).

2.6. Memory usage

No doubt, the main limitation of the approach is the memory

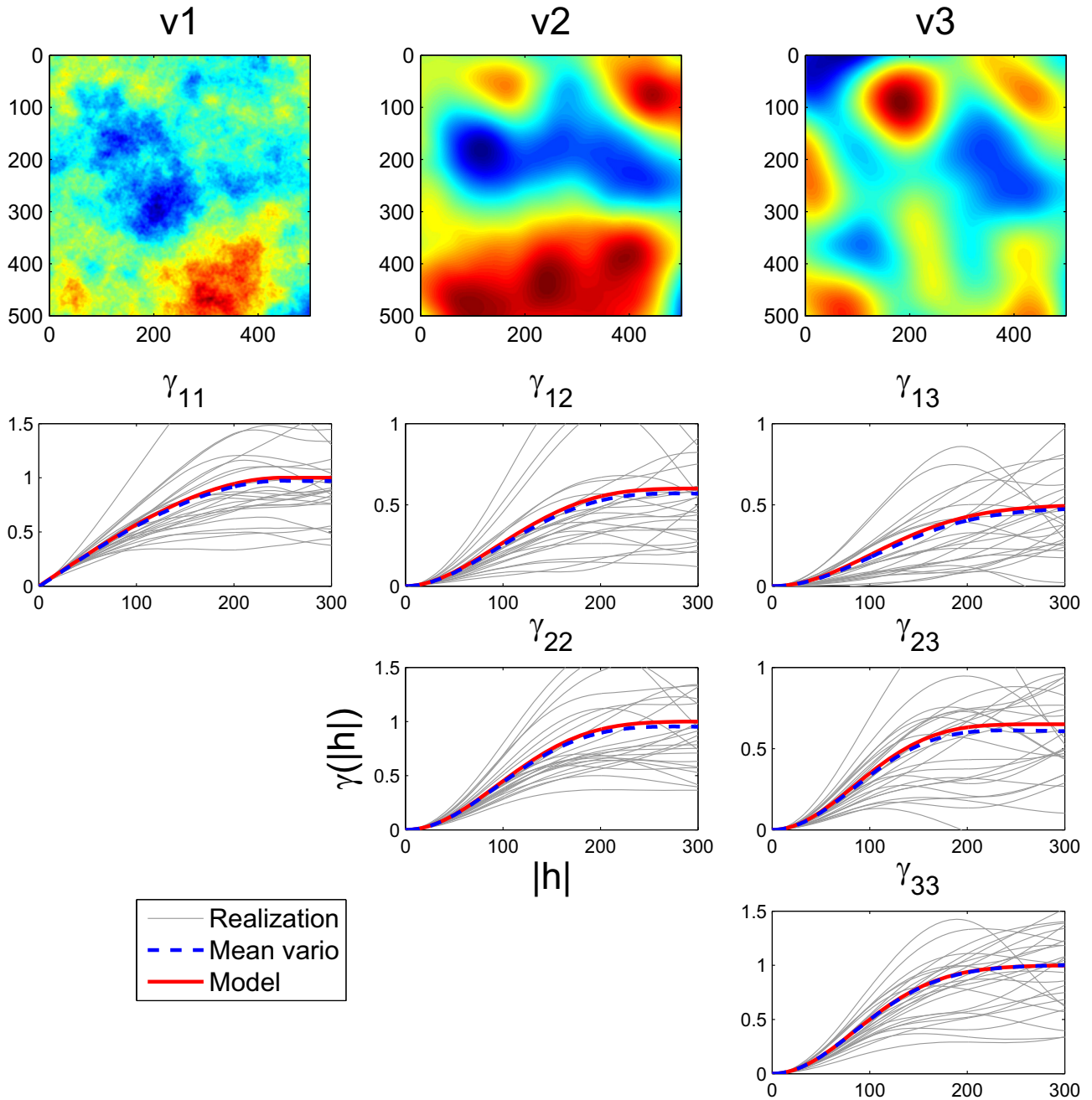


Fig. 4. One realization of v1, v2 and v3 (top row) and the direct and cross-variograms. Case 3 of Table 1. Mean variogram is computed by combining E–W and N–S directions over 200 realizations. Only the first 25 individual realization variograms (light gray) are shown.

usage, especially when simulating large grids for models with long practical range. The maximum memory mobilized by the current implementation of GFFTMA is approximately $32p^2(n_s + n_a)^d n_{sim}$, where p is the number of variables, n_s is the number of pixels simulated, n_a is the number of pixels required to reach the maximal practical range, d is the dimension of the studied field and n_{sim} is the number of realizations to simulate. Table 2 gives the approximate maximum size that can be simulated using only the available RAM memory in 2D and 3D as a function of memory available above the memory required to run the operating system and Matlab’s overhead. For larger fields, the program has to use a swap file, which slows considerably the execution time. Clearly, results of Table 2 indicate that GFFTMA is more suitable for simulation in 2D than in 3D, although mid-size problems in 3D can still be treated.

3. Case study – overburden thickness simulation

The case study bears on the cosimulation of overburden thickness and surface lithological information represented by a Gaussian latent variable. The overburden thickness data includes 4730 boreholes in Montérégie Est, in the south of Québec. The study area covers approximately 14,000 km² split into two main geological domains. The geological domain located at northwest (domain A) has generally higher overburden thickness than the rest (domain B). The sample locations are shown in Fig. 7.

A bivariate field is aimed to simulate by the GFFTMA. The logarithm of overburden thickness is treated as the first variable. Another known information is the indicator of geological domain of the studied area. A number of approaches can be used in the simulation of the geological types or facies, such as sequential

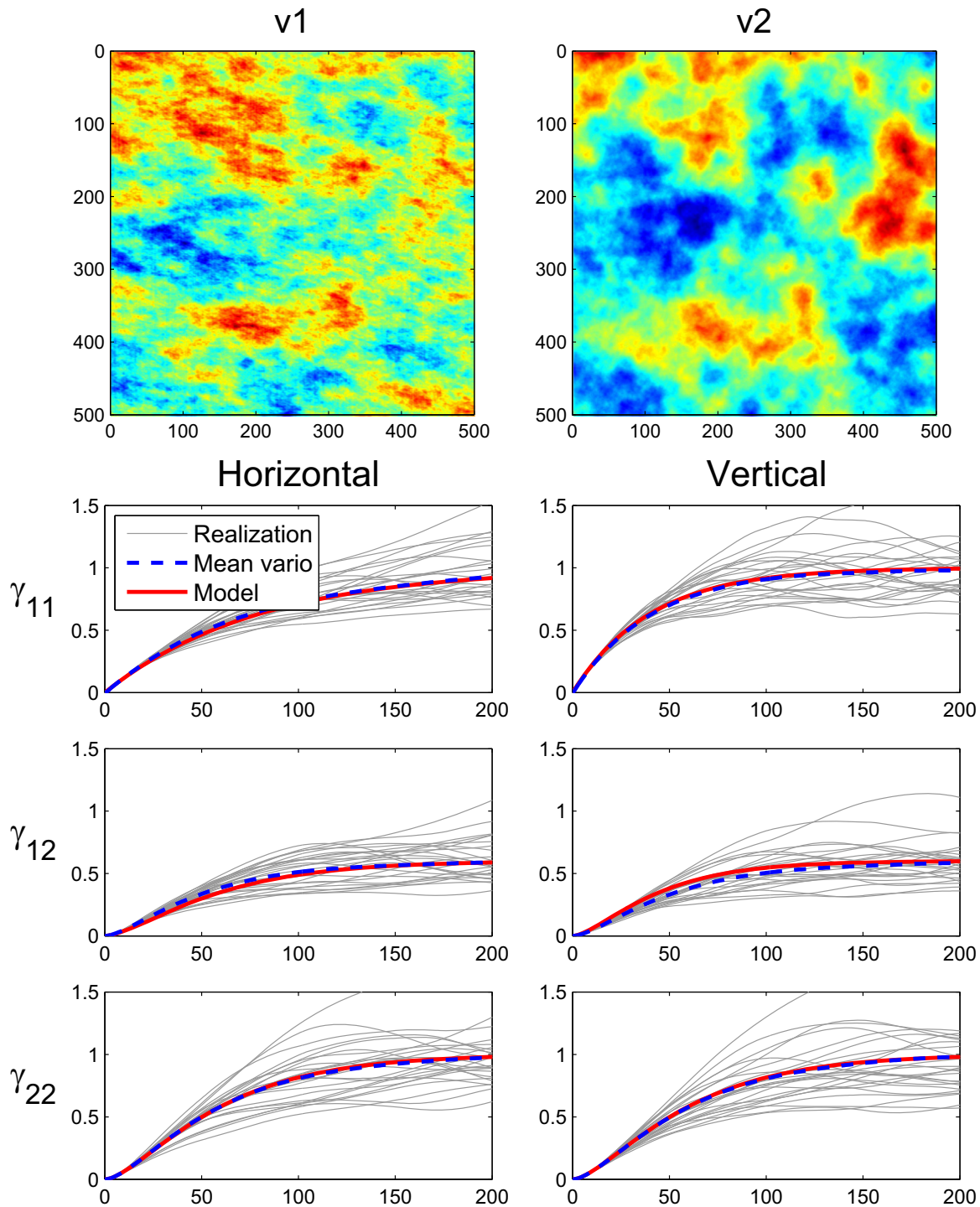


Fig. 5. One realization of v_1 and v_2 (top row) and the direct and cross-variograms. Case 4 (with geometric anisotropy) in Table 1. Horizontal direction (left column) and vertical direction (right column). Mean variogram is computed over 200 realizations. Light gray: variograms for the first 25 realizations.

indicator simulation (Journal and Isaaks, 1984; Deutsch and Journel, 1998), multiple point statistics (Guardiano and Srivastava, 1993; Ortiz and Deutsch, 2004), truncated Gaussian simulation (Matheron et al., 1987), and truncated pluriGaussian simulation (Galli et al., 1994). In this paper, we used the truncated Gaussian simulation, i.e. the geological domain indicator is obtained by thresholding a continuous latent Gaussian variable at the sampling points. First, the fixed threshold of the Gaussian field has been determined using declustered proportions of each geological domain. Then the latent variable variogram is chosen so as to match the indicator variogram and log(thickness)-indicator cross-

variogram. Having the variogram model of the latent variable, the Gibbs sampler provides latent Gaussian at sampling points in agreement with the geological domain indicator. For each conditional realization, a different Gibbs sampler realization of the latent Gaussian variable at sample points is used.

Fig. 8 shows the direct and cross variograms of the log(thickness) and the latent Gaussian variable. The experimental variogram of overburden log(thickness) is well adjusted by an exponential model. The latent variable was chosen to have a Gaussian covariance model because it provided better fit to the geological domain indicator variogram and log(thickness)-indicator

Table 1
Models used in Figs. 2–5 and 9.

Case	Figure	Model description
1	Fig. 2	v1–v1: Exponential ($a_p = 250, C = 1$) v1–v2: Cauchy ($a_p = 155, C = 0.6, \nu = 2$) v2–v2: K-Bessel ($a_p = 158, C = 1; \nu = 1$)
2	Fig. 3	v1–v1: Spherical ($a = 250, C = 1$) v1–v2: Cubic ($a = 310, C = 0.85$) v2–v2: Penta ($a = 350, C = 1$)
3	Fig. 4	v1–v1: Spherical ($a = 250, C = 1$) v1–v2: Cubic ($a = 310, C = 0.5$) v1–v3: Gaussian ($a_p = 250, C = 0.5$) v2–v2: Penta ($a = 350, C = 1$) v2–v3: Penta ($a = 310, C = 0.8$) v3–v3: Gaussian ($a = 208, C = 1$)
4	Fig. 5	v1–v1: Exponential ($a_{p,hor} = 240, a_{p,vert} = 120, C = 1$) v1–v2: K-Bessel ($a_{p,hor} = 158, a_{p,vert} = 118.5, C = 0.6, \nu = 1$) v2–v2: K-Bessel ($a_{p,iso} = 158, C = 1; \nu = 1$)
5	Fig. 9	v1–v1: Nugget ($C=0.15$)+Exponential ($a_p = 27 \text{ km}, C = 0.45$) v1–v2: Nugget($C=0.001$) + Gaussian ($a_p = 32.6 \text{ km}, C = 0.3$) v2–v2: Nugget($C=0.001$)+ Gaussian ($a_p = 24.6 \text{ km}, C = 1$)

cross-variogram. The fit obtained after the Gibbs sampling reproduces the assumed model as expected. Finally, the cross-variogram is also well fitted by a Gaussian model. Because the two variables have different direct variogram structures, they define a N-LMC model with zero-lag correlation of $R=0.38$.

Two series of unconditional realizations of logarithm of overburden thickness were obtained on a regular grid: an univariate simulation by FFTMA and the bivariate N-LMC simulation involving geological domain by GFFTMA. Then, the unconditional simulated values were extended to the sample point locations by local LU simulation.

Fig. 9 shows direct and cross variograms of the two variables for 30 unconditional realizations obtained in cosimulation of N-LMC. The average variograms of the 30 realizations coincide almost perfectly with the models. Each realization is then post-conditioned by cokriging using the same N-LMC model.

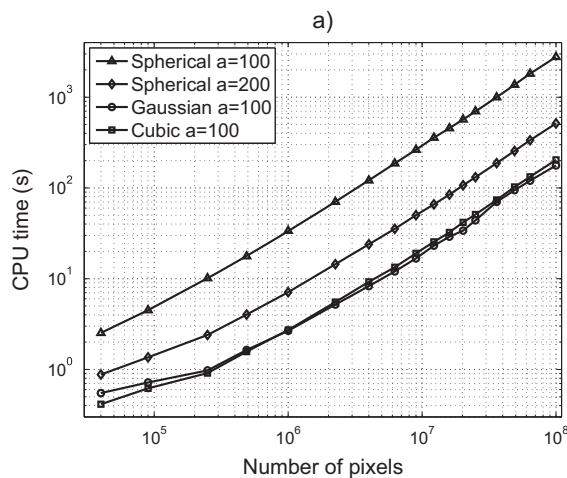


Table 2
Maximum size of simulated field as a function of available RAM above overhead memory required by operating system and Matlab (for $n_{sim} = 1, n_a = 100, p = 2$).

Available RAM	2D	3D
4G	5400 × 5400	210 × 210 × 210
16G	11,000 × 11,000	400 × 400 × 400
48G	19,000 × 19,000	620 × 620 × 620

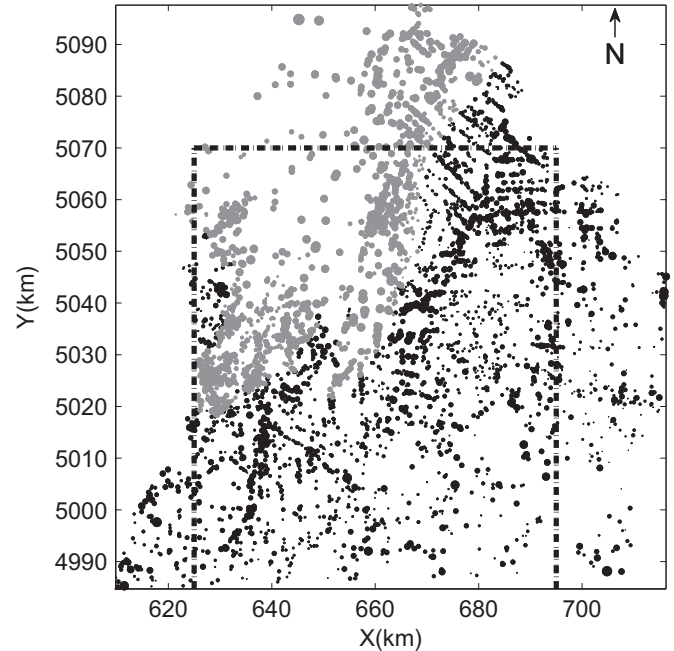


Fig. 7. Map of sample data. Gray dots: boreholes in geological domain A, black dots: boreholes in geological domain B. The area covered by simulation in Fig. 10 is outlined (dashed line).

3.1. Comparison of statistics of conditional realizations by N-LMC model and univariate simulation

To assess the gain obtained by considering the geological information, the full dataset is split into two parts: a small part (10%)

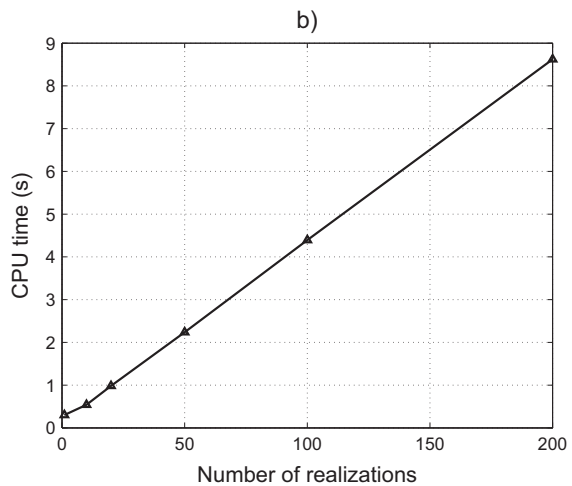


Fig. 6. Evolution of computing time as a function of (a) the number of simulated pixels and (b) the number of realizations (for a field of 200 × 200 pixels). Simulation of two variables for four different models in (a) and a spherical model with range 100 in (b).

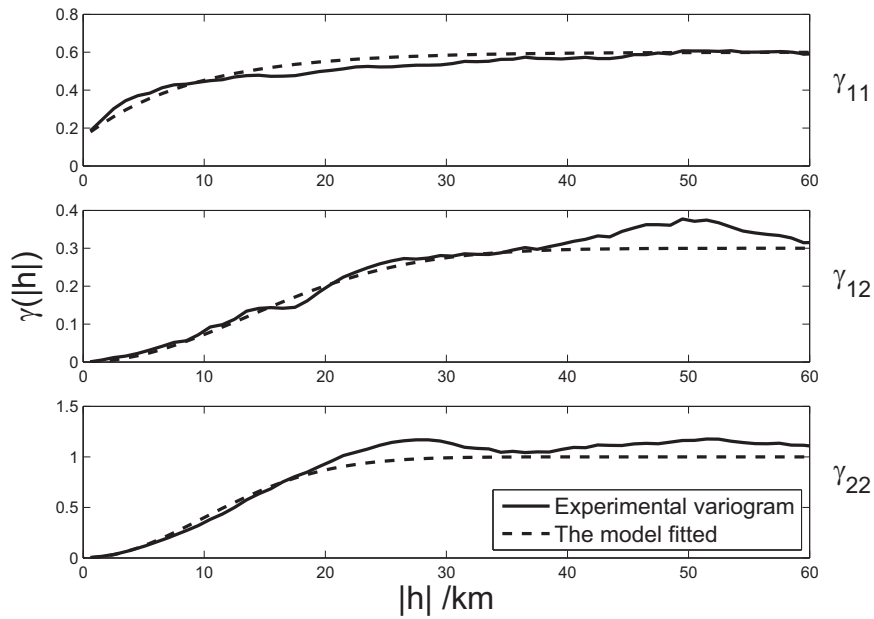


Fig. 8. Model fitting for direct and cross variograms of log(thickness) and one latent field representing the geological domain information.

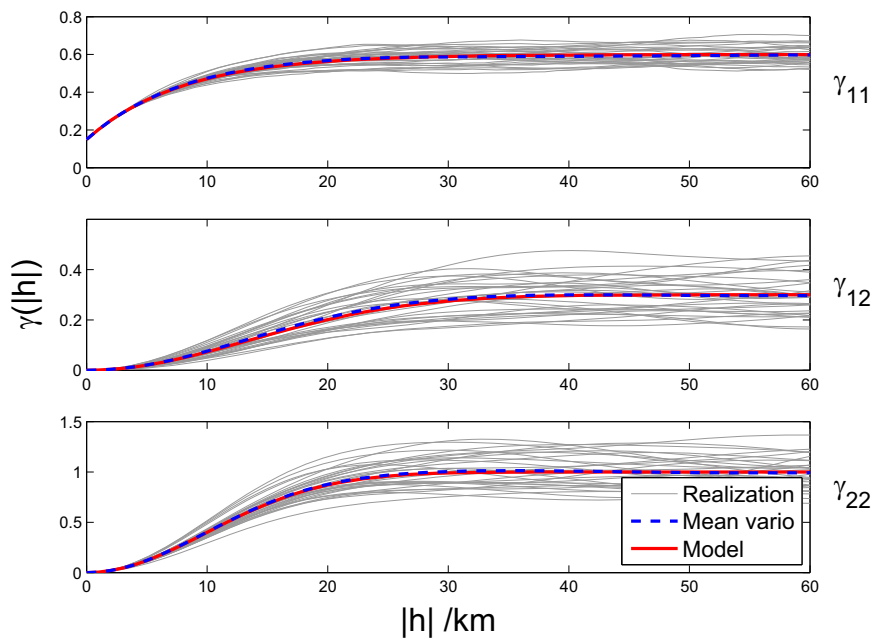


Fig. 9. Comparison of the direct and cross variograms of log(thickness) and the latent variable between 30 realizations and the theoretical model.

Table 3
Mean MAE (in m) for 30 realizations.

Simulation cases	On 981 testing points within 5 km distance from boundary	On all 4257 testing points
Case 1 (Univariate simulation)	6.49	6.95
Case 2 (N-LMC simulation)	6.21	6.68
% improvement with N-LMC	4.3	3.9

is used as conditioning data and the rest (90%) is used as test data. Conditional realizations are obtained at the test data locations for two different cases: one using the univariate simulation of log

(thickness) and the second using N-LMC simulation of log(thickness) with the Gaussian latent variable as secondary information at both conditioning points and test data locations. Then the final simulations of log(thickness) for overburden are transformed to the thickness. Table 3 shows mean statistics of 30 realizations obtained with the two instances. The mean absolute error (MAE) of simulation with N-LMC shows an improvement of 3.9% to 4.3% compared to the univariate simulation, indicating that despite the small zero-lag correlation ($R=0.38$), the geological information remains useful.

Fig. 10 shows 3 realizations of the univariate simulation (left) and the N-LMC (right), still using 10% of the thickness data and all the latent data. Clearly, the realizations of the N-LMC show larger thickness toward the North than do the univariate realizations.

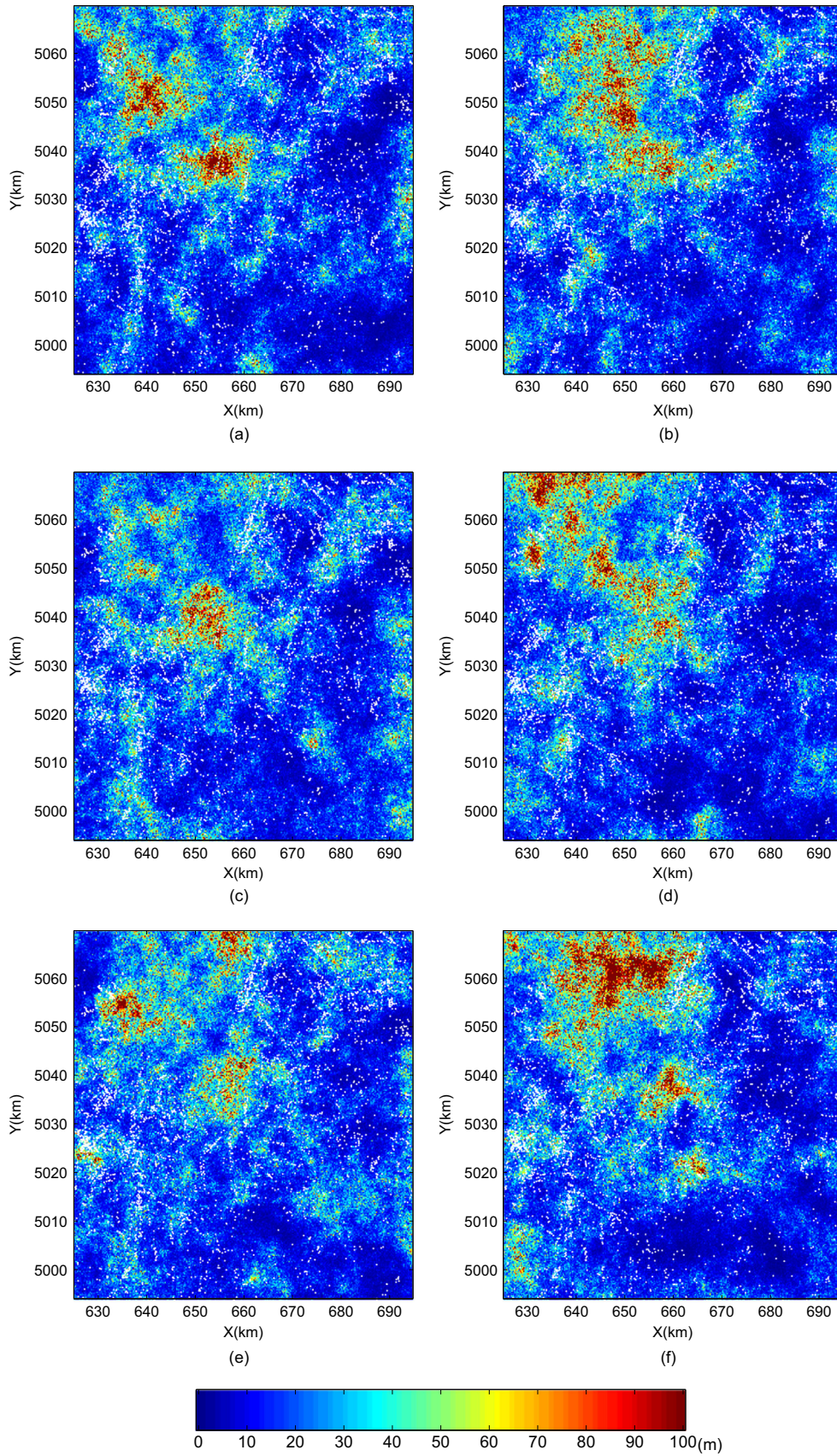


Fig. 10. Realizations of univariate simulation (left) and N-LMC simulation (right). White dots represent data locations.

Hence, one concludes that the geological information conveyed by the latent variable has a noticeable impact on the simulations despite the low correlation between the log(thickness) and the latent variable.

4. Discussion

Examples were provided illustrating simulation of the models available in GFFTMA. The average experimental direct and cross-variograms reproduced almost perfectly the theoretical model in all cases presented (see Figs. 2–5) even for N-LMC known to be not strictly admissible like the N-LMC models having a compactly supported direct covariance function (e.g. models in Figs. 3 and 4). These models are known to be non-admissible (Marcotte, 2015), because at high frequencies the spectral densities of the compactly supported covariance function possess multiple zeros, hence the spectral density matrix cannot be positive semidefinite at these frequencies. However, this fact has little consequence in practice as seen by the quality of the reproduction of all direct and cross-covariances. Moreover, the adopted correction for the small negative eigenvalues renders these models admissible at the sampled scale. In the post-conditioning by cokriging, there were no instance where the cokriging matrix was found not positive definite.

The eigen-decomposition is done at each frequency where the amplitude exceeds the threshold $A_{max,i}/10^6$, where $A_{max,i}$ is the maximum amplitude found in the direct spectrum of variable i . As soon as one threshold is exceeded, the spectral matrix is eigen-decomposed. As a consequence, the CPU times of GFFTMA are largely related to the behavior at the origin of the models present in the N-LMC. Linear behavior variograms have larger high frequencies, hence eigen-decomposition must be computed at more frequencies. For the same behavior at the origin, the smaller the range with respect to simulated field size, the larger the CPU time. Nevertheless, the CPU times remain tractable and always keep the $N \log(N)$ dependency, where N is the number of pixels to simulate. Moreover, the eigen-decomposition is done only once, irrespective of the number of realizations. Previous trials with the Cholesky decomposition, instead of eigen-decomposition, to compute the square root matrices were significantly faster but proved numerically unstable in many circumstances. For this reason, it is preferable to stick to the slower eigen-decomposition.

The memory requirements are rather important as the field size to simulate internally in GFFTMA to reduce aliasing is equal to the size of the field to simulate plus the maximal practical range found among all model components. As an example, with a maximal practical range of 100, 48G of RAM enables simulation of a field comprising approximately 238 million pixels in 3D, corresponding to 620 pixels along each dimension. One avenue to limit the size of the simulation may be to try to approximate models displaying asymptotic sills (exponential, Gaussian, Cauchy and K-Bessel) by combination of models with compact support (spherical, cubic and penta). This could reduce significantly the size of the field to simulate internally, although it is not clear if the number of frequencies to eigen-decompose does also diminish.

5. Conclusion

The GFFTMA program can generate unconditional simulations in both isotropic and anisotropic situations for any number of variables and any number of covariance components for each direct and cross-covariances. It enables us to simulate N-LMC with symmetric cross-covariances. Basic covariance models included in

GFFTMA are nugget, exponential, Gaussian, spherical, cubic, penta, generalized Cauchy and K-Bessel (Matérn). If needed, other models can be added easily with a single line of code. Simulated examples show that GFFTMA succeed to produce realizations having on average the desired N-LMC.

Acknowledgments

This research was financed by NSERC (RGPIN-2015-06653) and by Polytechnique Montral. The constructive comments of three anonymous reviewers were helpful to improve the manuscript.

Appendix A. Usage of GFFTMA

The program GFFTMA is a Matlab function used to produce unconditional simulations of N-LMC models. For conditional simulation, it must be completed with other functions performing 1-extension of the unconditional grid to sample points not lying on the grid and 2-the post-conditioning by cokriging with the same N-LMC model. The check of the admissibility of the N-LMC model can be done with program TASC3D (Marcotte, 2015).

GFFTMA is called with :

```
datasim = gffتما(model,seed,nsim,vsiz,grid,thres)
```

The input *model* is a cell variable of size $n \times n$, n being the number of variables. Each model $\{i, j\}$ possesses p_{ij} elementary components. As GFFTMA assumes symmetric cross-covariances, model $\{i, j\}$ must be the same as model $\{j, i\}$. Each component is specified with 4 parameters (when all components of all models are isotropic) or 6 parameters in the 2D anisotropic case and 9 parameters in the 3D anisotropic case. In the isotropic case, the four parameters are 1-model type, 2-range, 3-shape, 4-sill. In the 2D anisotropic case, the 6 parameters are 1-model type, 2-first range, 3-second range, 4-anticlockwise rotation, 5-shape parameter and 6-sill. In the 3D anisotropic case, the 9 parameters are 1-model type, 2-first range, 3-second range, 4-third range, 5-rotation around x , 6-rotation around y , 7 rotation around z , 8-shape, and 9-sill. The shape parameter is used only for model types 7 (Cauchy) or 8 (K-Bessel). The rotations follow the same convention and order as described in Marcotte (1991), i.e. all anticlockwise rotations, z first, then y , then x . The model types are 1-nugget, 2-exponential, 3-Gaussian, 4-spherical, 5-cubic, 6-penta, 7-Cauchy 8-K-Bessel. As soon as one model component is anisotropic, all models (even isotropic ones) must be specified with the anisotropic convention.

The input *seed* is the seed of the random number generator.

The input *nsim* is the number of realizations required.

The input $1 \times d$ vector *vsiz* allows the user to specify the number of pixels to use internally for the simulation. This enables us to fix the random numbers to the same values for two different calls to GFFTMA by specifying the same seed and the same *vsiz*. The internal number of pixels must be chosen so as to prevent aliasing, i.e. it must be larger than practical range (in pixels) plus the desired size (in pixels) to simulate. Normal usage is to leave this vector empty. The program then computes the required number of pixels.

The input *grid* is a vector. In 1D it contains $[nx, dx]$, in 2D it contains $[nx, dx, ny, dy]$ and in 3D $[nx, dx, ny, dy, nz, dz]$, where nx is the number of pixels desired in the x direction and dx is the distance between consecutive pixels along x , and similarly for directions y and z .

The input *thres* is the multiplying factor applied to the maximal spectral density value. The spectral matrices where

$S_i(f) > \text{thres} * \max_j S_j(f)$ for at least one i are eigen-decomposed. When *thres* is left empty, the default value $\text{thres} = 10^{-6}$ is used. Using larger values reduces the number of required eigen-decompositions and thus speeds up the simulation but it may affect the correct reproduction of the linear behavior at short distances of the exponential and spherical models.

The output *datasim* is a cell array of size $nsim \times nvar$ with the results of the simulation.

References

- Ahmed, S., de Marsily, G., 1989. Co-kriged estimates of transmissivities using jointly water level data. In: Armstrong, M. (Ed.), *Geostatistics. Quantitative Geology and Geostatistics vol. 4*. Springer, Netherlands, pp. 615–628, URL <http://dx.doi.org/10.1007/978-94-015-6844-9-48>.
- Asli, M., Marcotte, D., Chouteau, M., 2000. Direct inversion of gravity data by cokriging. In: Kleingeld, W.J., Krige, D.G. (Eds.), *Geostatistics 2000*, Cape Town, South Africa, pp. 64–73.
- Chilès, J.-P., 1995. Quelques méthodes de simulation de fonctions aléatoires intrinsèques. *Cahiers de Géostatistique*, Fasc. vol. 5, pp. 97–112.
- Chilès, J.-P., Delfiner, P., 1997. Discrete exact simulation by the Fourier method. In: Baafi, E. (Ed.), *Geostatistics, Wollongong*, vol. 96, pp. 258–269.
- Chilès, J.-P., Delfiner, P., 2012. *Geostatistics: Modeling Spatial Uncertainty*. John Wiley & Sons, New York.
- Cooley, J.W., Lewis, P.A., Welch, P.D., 1969. The fast Fourier transform and its applications. *IEEE Trans. Educ.* 12 (1), 27–34.
- Davis, M., Grivet, C., 1984. Kriging in a global neighborhood. *Math. Geol.* 16, 249–265.
- Deutsch, C.V., Journel, A.G., 1998. *GSLIB—Geostatistical Software Library and User's Guide*. Oxford University Press, New York.
- Dong, A., 1990. Estimation géostatistique des phénomènes régis par des équations aux dérivées partielles (PhD thesis). Centre de géostatistique, Fontainebleau.
- Emery, X., 2007. Conditioning simulations of Gaussian random fields by ordinary kriging. *Math. Geol.* 39 (6), 607–623.
- Emery, X., Arroyo, D., Porcu, E., 2015. An improved spectral turning-bands algorithm for simulating stationary vector Gaussian random fields. *Stoch. Environ. Res. Risk Assess.*, in press. URL <http://dx.doi.org/10.1007/s00477-015-1151-0>.
- Galli, A., Beucher, H., Le Loch, G., Doligez, B., et al., 1994. The pros and cons of the truncated Gaussian method. In: *Geostatistical Simulations*. Springer, Dordrecht, pp. 217–233.
- Gloaguen, E., Marcotte, D., Chouteau, M., Perroud, H., 2005. Borehole radar velocity inversion using cokriging and cosimulation. *J. Appl. Geophys.* 57 (4), 242–259.
- Goulard, M., Voltz, M., 1992. Linear coregionalization model: tools for estimation and choice of cross-variogram matrix. *Math. Geol.* 24 (3), 269–286, URL <http://dx.doi.org/10.1007/BF00893750>.
- Guardiano, F.B., Srivastava, R.M., 1993. Multivariate geostatistics: beyond bivariate moments. In: *Geostatistics Troia92*. Springer, Dordrecht, pp. 133–144.
- Journel, A., Isaaks, E., 1984. Conditional indicator simulation: application to a Saskatchewan uranium deposit. *Math. Geol.* 16 (7), 685–718.
- Journel, A.G., 1974. Geostatistics for conditional simulation of ore bodies. *Econ. Geol.* 69 (5), 673–687.
- Journel, A.G., Huijbregts, C.J., 1978. *Mining Geostatistics*. Academic Press, London.
- Le Ravalec-Dupin, M., Da Veiga, S., 2011. Cosimulation as a perturbation method for calibrating porosity and permeability fields to dynamic data. *Comput. Geosci.* 37 (9), 1400–1412.
- Le Ravalec-Dupin, M., Hu, L., Noetinger, B., 2001. Stochastic reservoir modeling constrained to dynamic data: local calibration and inference of structural parameters. *SPE J.* 6 (01), 25–31.
- Le Ravalec-Dupin, M., Noetinger, B., Hu, L., 2000. The FFT moving average generator: an efficient numerical method for generating and conditioning Gaussian simulations. *Math. Geol.* 32, 701–722.
- Mantoglou, A., 1987. Digital simulation of multivariate two- and three-dimensional stochastic processes with a spectral turning bands method. *Math. Geol.* 19 (February (2)), 129–149.
- Marcotte, D., 1991. Cokriging with Matlab. *Comput. Geosci.* 17, 1265–1280.
- Marcotte, D., 2015. TASC3D: a program to test the admissibility in 3d of non-linear models of coregionalization. *Comput. Geosci.* 83, 168–175, URL (<http://www.sciencedirect.com/science/article/pii/S0098300415300194>).
- Matheron, G., 1973. The intrinsic random functions and their applications. *Adv. Appl. Probab.* 5 (3), 439–468.
- Matheron, G., Beucher, H., De Fouquet, C., Galli, A., Guerillot, D., Ravenne, C., 1987. Conditional simulation of the geometry of fluvio-deltaic reservoirs. *Paper SPE*, vol. 16753, pp. 22–25.
- Mejía, J.M., Rodriguez-Iturbe, I., 1974. On the synthesis of random field sampling from the spectrum: an application to the generation of hydrologic spatial processes. *Water Resour. Res.* 10 (4), 705–711.
- Myers, D., 1983. Estimation of linear combinations and co-kriging. *Math. Geol.* 15 (5), 633–637, URL <http://dx.doi.org/10.1007/BF01093416>.
- Oliver, D.S., 1995. Moving averages for Gaussian simulation in two and three dimensions. *Math. Geol.* 27 (8), 939–960.
- Oliver, D.S., 2003. Gaussian cosimulation: modelling of the cross-covariance. *Math. Geol.* 35, 681–698.
- Ortiz, J.M., Deutsch, C.V., 2004. Indicator simulation accounting for multiple-point statistics. *Math. Geol.* 36 (5), 545–565.
- Pardo-Igúzquiza, E., Chica-Olmo, M., 1993. The Fourier integral method: an efficient spectral method for simulation of random fields. *Math. Geol.* 25 (2), 177–217.
- Priestley, M., 1982. Spectral analysis and time series. In: *Probability and Mathematical Statistics*, vols. 1–2. Academic Press, San Diego. URL (<https://books.google.ca/books?id=bHxGAAAYAAJ>).
- Rao, K.R., Kim, D.N., Hwang, J.J., 2011. *Fast Fourier Transform-Algorithms and Applications*. Springer Science & Business Media, Dordrecht.
- Royer, J.J., Vieira, P., 1984. Dual formalism of kriging. In: Verly, G., David, M., Journel, A.G., Marechal, A. (Eds.), *Geostatistics for Natural Resources Characterization, Part 2*. NATO-ASI, pp. 691–702.
- Shamsipour, P., Chouteau, M., Marcotte, D., 2011. 3D stochastic inversion of magnetic data. *J. Appl. Geophys.* 73 (4), 336–347.
- Shamsipour, P., Marcotte, D., Chouteau, M., Keating, P., 2010. 3D stochastic inversion of gravity data using cokriging and cosimulation. *Geophysics* 75, 11–110.
- Shinozuka, M., 1971. Simulation of multivariate and multidimensional random processes. *J. Acoust. Soc. Am.* 49 (1B), 357–368.
- Shinozuka, M., Jan, C.M., 1972. Digital simulation of random processes and its applications. *J. Sound Vib.* 25 (1), 111–128.
- Wackernagel, H., 2003. *Multivariate Geostatistics*, 2nd edition. Springer Science & Business Media, Berlin.
- Zagayevskiy, Y., 2015. *Multivariate Grid-Free Geostatistical Simulation of Natural Phenomena* (PhD thesis). University of Alberta, Edmonton.